Optical and Quantum Electronics (2026) 58:42
https://doi.org/10.1007/s11082-025-08635-w

# Quantitative assessment of the self-healing phenomenon in Hermite–Gauss beams using intensity- and amplitude-based similarity metrics

**Rafie Rafie Zadeh[1] · Abdollah Borhanifar[1] · Pari Amiri[2] · Yashar Azizian-Kalandaragh[3,4,5]**

Received: 26 October 2025 / Accepted: 11 December 2025


**Abstract**
The ability of structured light to reconstruct after partial obstruction, known as the self-healing phenomenon, has attracted considerable attention for applications in imaging, optical communication, and quantum technologies. While Bessel and Airy beams have been extensively studied, the self-healing behavior of Hermite–Gauss (HG) beams remains less well quantified. In this work, we systematically investigate the self-healing properties of six HG modes ($HG_{01}$, $HG_{10}$, $HG_{11}$, $HG_{12}$, $HG_{21}$, $HG_{22}$) under three classes of obstructions: circular disks, vertical strips, and rectangular fringes. Both intensity- and amplitude-based similarity measures are employed within the normalized self-healing degree (SHD) framework, providing a rigorous and comparable metric of recovery efficiency. Numerical simulations reveal that higher-order modes, particularly $HG_{22}$, demonstrate superior resilience, achieving SHD values above 1.1 even for moderate obstructions, whereas lower-order modes exhibit incomplete recovery. Geometry–mode alignment effects are also observed, with $HG_{11}$ showing enhanced robustness under strip obstructions. Importantly, amplitude-based SHD is consistently lower than intensity-based SHD, confirming that apparent intensity recovery can overestimate robustness when phase fidelity is critical. These findings establish a comprehensive quantitative picture of HG self-healing and offer practical insights for designing resilient, structured beams in realistic optical environments.

**Keywords** Structured light · Hermite–Gauss beams · Self-healing phenomenon · Normalized similarity measure · Amplitude and intensity recovery

✉ Yashar Azizian-Kalandaragh
yashar.a.k@gmail.com

[1] Department of Mathematics, University of Mohaghegh Ardabili, P.O. Box 179, Ardabil, Iran

[2] Department of Engineering Sciences, Faculty of Advanced Technologies, Sabalan University of Advanced Technologies (SUAT), Namin, Iran

[3] Department of Physics, University of Mohaghegh Ardabili, P.O. Box 179, Ardabil, Iran

[4] Department of Photonics, Faculty of Applied Sciences, Gazi University, 06500 Ankara, Turkey

[5] Photonics Application and Research Center, Gazi University, 06500 Ankara, Turkey

Published online: 18 December 2025

## 1 Introduction

Structured light, which is an optical field whose spatial amplitude, phase, or polarization is engineered, has become a key tool in imaging, optical communication, and manipulation (Forbes 2019; Forbes et al. 2021; Angelsky et al. 2020). Among its fascinating properties is self-healing, in which a beam recovers its profile (shape and/or intensity) after passing an obstacle, even though part of the field was blocked. Early foundational work on nondiffracting beams, especially Bessel and Bessel-Gaussian beams, established that beams with large angular spectrum support can reconstruct behind obstructions (Wen and Chu 2015; Arrizón et al. 2015). Accelerating beams, such as Airy beams, also exhibit this behavior in both theory and experiment, including the recovery of main lobes after severe obstruction (Broky et al. 2008).

Quantification has increasingly become central. Similarity metrics, including normalized overlap, root-mean-square error, and correlation, have been used to define recovery as a function of distance along the propagation path (Chu and Wen 2014). More recently, amplitude-based measures have been proposed because intensity-only measures can understate or misrepresent the extent to which the wavefront (phase and structure) is recovered (Aiello et al. 2017). Zhao et al. studied the self-healing and structural transformation of obstructed Hermite-Gaussian modes, showing when and how HG modes can reconstruct or degrade into lower-order modes, depending on the obstruction and retained features (Zhao et al. 2023). Saadati-Sharafeh et al. (2023) introduce an improved similarity-based SHD metric that normalizes by the initial distortion, enabling comparisons across beam types and obstruction strengths (Saadati-Sharafeh et al. 2023).

Hermite-Gauss modes ($HG_{mn}$) are of special interest because their nodal structure introduces symmetry axes and interference in a Cartesian framework; mode order influences how much energy is in sidelobes and how quickly the angular spectrum can reconstruct blocked parts (Xu et al. 2020). Existing studies have begun to uncover some mode-dependent behavior, but these often lack systematic size/geometric obstacle sweeps, or amplitude-vs-intensity metric comparisons, or normalization relative to initial distortion (Zhao et al. 2023; Xu et al. 2020). In addition, although Elegant Gaussian beams (HG-type and LG-type) have been compared to pseudo-nondiffracting beams for obstruction recovery, the studies often focus on lower-order or symmetric modes (Chabou and Bencheikh 2020).

This work addresses these gaps. We perform full numerical simulations of multiple Hermite-Gauss modes, specifically $HG_{10}$, $HG_{01}$, $HG_{11}$, $HG_{12}$, $HG_{21}$, and $HG_{22}$, subject to several canonical obstruction shapes and sizes. We compute normalized SHD metrics both intensity-based and amplitude-based, plot SHD vs. z, show intensity profile recovery, and build comparative tables to reveal how mode order, obstacle type, and size affect the maximum recovery and distance at which recovery occurs. The results are intended not just to characterize, but to guide the design of structured light in applications where occlusion or partial obstruction is common, such as imaging through scattering media or optical communication.

## 2 Methods

### 2.1 Beam model: Hermite–Gauss modes

Hermite–Gauss (HG) modes form a complete set of solutions to the paraxial wave equation in Cartesian coordinates and are widely used in laser resonator theory, free-space optics, and mode-division multiplexing (Siegman and Lasers 1986; Bandres and Gutiérrez-Vega 2004). The transverse field distribution of the $HG_{mn}$ mode at the beam waist plane is given by (Gutiérrez-Vega and Bandres 2005):

$$U_{m,n}(x,y,0) = H_m\left(\frac{\sqrt{2}x}{w_0}\right) H_n\left(\frac{\sqrt{2}y}{w_0}\right) \exp\left(-\frac{x^2+y^2}{w_0}\right) \tag{1}$$

Where $H_m$ and $H_n$ are Hermite polynomials of order m and n, and $w_0$ is the waist radius. In this study, $w_0$ was fixed at 0.30 mm to match typical laboratory-scale Gaussian beams (Kogelnik and Li 1966). Six modes were selected, i.e., $HG_{10}$, $HG_{01}$, $HG_{11}$, $HG_{12}$, $HG_{21}$, and $HG_{22}$, to cover asymmetric, symmetric, and higher-order distributions. It is worth noting that, in addition to their theoretical role, first-order modes such as $HG_{10}$ and $HG_{01}$ are used in practice to generate vortex beams (Laguerre–Gaussian) using astigmatic converters; this conversion allows the generation of beams carrying angular momentum (OAM) and is useful in spaceborne communications, particle manipulation, and some materials processing applications (Beijersbergen et al. 1993; Uren et al. 2019).

### 2.2 Propagation model: angular spectrum method

To model free-space propagation, the angular spectrum method was employed, which provides a numerically exact solution of the scalar Helmholtz equation without paraxial approximations (Goodman 2005; Voelz 2011). The propagated field is given by (Goodman 2005):

$$U(x,y,z) = \mathcal{F}^{-1}\left\{\mathcal{F}\left[U(x,y,0)\right] \exp\left[ik_z\left(f_x,f_y\right)z\right]\right\} \tag{2}$$

where $\mathcal{F}$ denotes the Fourier transform, $(f_x, f_y)$ are spatial frequencies, and

$$k_z = \sqrt{k^2 - \left(2\pi f_x\right)^2 - \left(2\pi f_y\right)^2} \tag{3}$$

Here, $k = 2\pi/\lambda$ is the free-space wavenumber at the He-Ne wavelength of $\lambda = 633\,nm$. A computational grid of $128 \times 128$ points spanning a 4 mm aperture was used, corresponding to a sampling interval of 31.25 µm, which satisfies the Nyquist criterion for the chosen beam waist and obstruction sizes. Propagation distances up to 200 mm were considered, discretized into 41 steps to provide adequate longitudinal resolution.

### 2.3 Obstruction models

Beam self-healing is inherently linked to how spatial frequencies bypass and reconstruct after an obstacle (Broky et al. 2008; Shen et al. 2022). To probe robustness under different scenarios, three canonical obstruction geometries were imposed on the waist plane: (I) Circular disk: a centered opaque disk of radius r, modeling symmetric localized blockage. (II) Vertical strip: an opaque band of half-width r centered on the beam axis, simulating partial aperture or slit obstruction. (III) Rectangular fringe: a vertical rectangular obstacle of half-width r and fixed half-height 180 μm, representing elongated occlusions such as wires or edges.

For each geometry, radii of 0.05 mm, 0.15 mm, and 0.25 mm were tested, corresponding to weak, moderate, and strong perturbations relative to the beam waist.

### 2.4 Similarity metrics and self-healing degree

Quantifying self-healing requires robust similarity measures between obstructed and unobstructed fields. Based on refs (Wen and Chu 2015; Aiello et al. 2017), we adopted the normalized similarity function:

$$S(A,B) = \left(1 - \sqrt{\frac{\|A-B\|^2}{\|A+B\|^2}}\right) \times 100\% \tag{4}$$

where A and B denote either the intensity distributions ($|U|^2$) or the complex amplitudes (U), and the norm is taken over a circular region of interest (ROI) of radius $1.5w_0$. Two variants were implemented:

(I) Intensity similarity: sensitive to envelope recovery,
(II) Amplitude similarity: accounts for both amplitude and phase recovery (Aiello et al. 2017).

The self-healing degree (SHD) was defined as (Saadati-Sharafeh et al. 2023):

$$SHD(z) = \frac{S(A(z), B(z))}{S(A(0), B(0))} \tag{5}$$

so that SHD > 1 indicates improved recovery relative to the initial obstructed plane. This normalization corrects for trivial similarity at z=0 and enables reproducible comparisons across obstruction sizes and beam families.

### 2.5 Simulation outputs and analysis

For each HG mode and obstruction condition, the beam evolution was qualitatively and quantitatively determined. To provide an intuitive picture of the reconstruction process, two-dimensional intensity distributions of the reference and obstructed beams were recorded at

selected propagation distances (0, 100, 200 mm). These snapshots allow direct visual comparison of how different modes respond to increasing propagation after obstruction.

Moreover, the normalized SHD for both intensity-based and amplitude-based similarity metrics as functions of propagation distance was plotted. From these curves, the maximum SHD values and the corresponding optimal propagation distances were extracted. To facilitate systematic comparison, all results were compiled into summary tables that report recovery performance across mode orders, obstruction types, and obstacle sizes. The combination of intensity maps, SHD curves, and comparative tables provides a comprehensive picture of the self-healing behavior of HG beams.

## 3 Results and discussion

### 3.1 Intensity evolution of HG modes

Figure 1 illustrates the transverse intensity distributions of selected Hermite-Gauss modes with and without obstruction at representative propagation distances (0, 100 mm, and 200 mm). The visual comparison immediately confirms the expected dependence of self-healing on both mode order and obstruction geometry. Lower-order modes such as $HG_{10}$ are most vulnerable to central obstruction by a circular disk, as their intensity is concentrated around the axis. Even after 200 mm of propagation, their core remains severely depleted, and the original nodal structure is only weakly recovered.

It is worth noting that third-order modes, such as $HG_{12}$ and $HG_{21}$, are particularly useful for applications including multi-particle optical trapping, structured illumination in imaging, and optical lithography due to their intensity multi-lobe structure, due to the energy distribution between the lobes, which is crucial for controlling the absorption/radiation force mechanism (Otte and Denz 2020; Sundin et al. 2024; Zhou et al. 2018). Moreover, the fourth-order mode, i.e., $HG_{22}$, retains more peripheral lobes after obstruction, which later diffract inward and contribute to the reconstruction of the central region. This qualitative behavior echoes earlier reports that self-healing is strongly correlated with redundancy in the beam's angular spectrum (Wen and Chu 2015; Aiello et al. 2017).

The asymmetry of strip and rectangular obstructions generates distinct recovery pathways. For strip-shaped masks, $HG_{11}$ exhibits relatively better resilience than $HG_{10}$, since its natural diagonal nodal line partially overlaps with the blocked region, reducing effective energy loss. This strip obstruction resistance property of $HG_{11}$ suggests that this mode could be a suitable choice for communication channels or systems in which strip masks (e.g., wires or edges) appear periodically; also, due to its nodal structure, $HG_{11}$ is used in mode sorting/detection methods and in MDM systems (Sundin et al. 2024; Zhou et al. 2018; Hofer et al. 2019).

Rectangular masks, on the other hand, introduce diffraction sidelobes that mimic higher-order lobes but lack coherence with the original beam. As a result, apparent structural recovery in intensity maps is deceptive; quantitative analysis below reveals that SHD values for fringe obstructions remain close to unity, indicating negligible true self-healing.


**Fig. 1** Transverse intensity profiles of selected HG modes ($HG_{01}$, $HG_{10}$, $HG_{11}$, $HG_{12}$, $HG_{21}$, and $HG_{22}$) at three propagation distances (0, 100 mm, and 200 mm). Obstructions: disk of radius 0.15 mm, vertical strip of half-width 0.15 mm, rectangular fringe of half-width 0.15 mm

### 3.2 Normalized SHD curves

To quantify the degree of reconstruction, the normalized SHD was calculated using both intensity-based and amplitude-based similarity metrics, as defined in Sect. 2.4. Figures 2, 3 and 4 present SHD as a function of propagation distance for $HG_{10}$, $HG_{11}$, and $HG_{22}$ modes across three obstruction types, respectively. At the waist plane (z=0), all curves are normalized to unity by definition. With propagation, amplitude-based SHD increases as unblocked angular spectrum components diffract around the obstacle and interfere to restore the field.

Several clear patterns emerge. First, higher-order modes consistently achieve greater recovery than lower-order ones. For example, $HG_{22}$ mode reaches SHD values above 1.1 under disk obstruction (see Fig. 4), while $HG_{10}$ mode saturates close to unity at the intensity-based metric. This confirms that the redundancy of multiple lobes provides more spectral information for reconstruction, in line with theoretical predictions (Aiello et al. 2017; Saa-

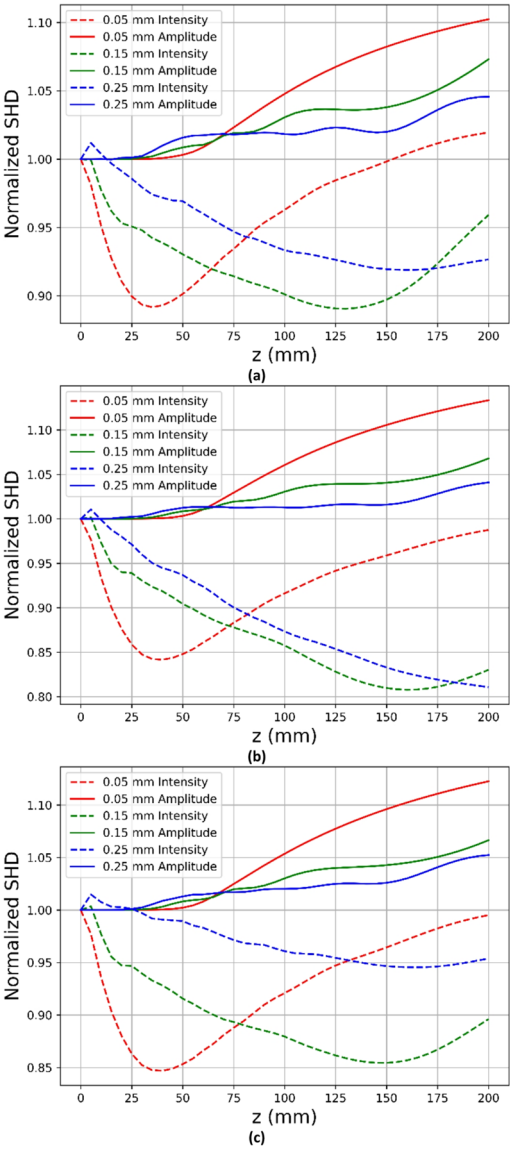


**Fig. 2** The SHD curves for $HG_{10}$ modes obstructed by a **a** disk, **b** vertical strip, and **c** rectangle with different sizes. Red dashed lines correspond to intensity-based similarity; blue solid lines correspond to amplitude-based similarity

dati-Sharafeh et al. 2023). The higher recovery observed for $HG_{22}$ suggests that this mode could be a desirable choice in mode-division and free-space optical communication systems requiring stability in the presence of partial obstruction. Additionally, higher-order modes have attracted attention in certain precision optical systems, such as those proposed for noise reduction in high-sensitivity detection systems (Nimavat et al. 2023; Ast et al. 2021).

Second, obstruction size strongly influences the achievable SHD. With small disks (0.05 mm), recovery is strong, and normalized SHD exceeds 1.0 in some cases, demonstrating nearly complete reconstruction. With larger obstructions (0.25 mm), recovery is weak or absent, and SHD plateaus near 1.0. This behavior highlights the physical limits

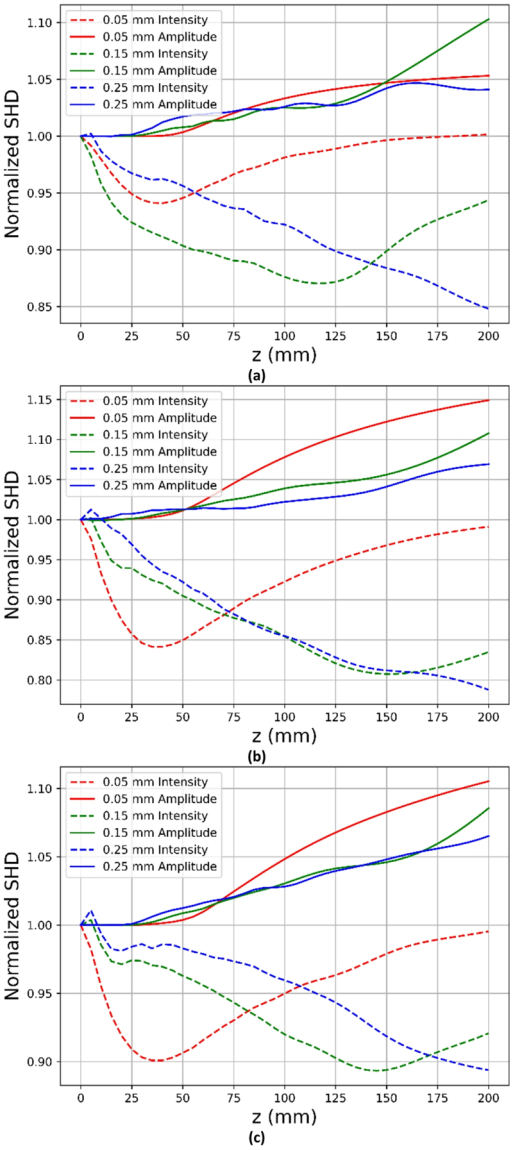


**Fig. 3** The SHD curves for $HG_{11}$ modes obstructed by a **a** disk, **b** vertical strip, and **c** rectangle with different sizes. Red dashed lines correspond to intensity-based similarity; blue solid lines correspond to amplitude-based similarity

of self-healing: once too much of the beam's angular spectrum is removed, no meaningful reconstruction is possible.

A consistent feature across all cases is the discrepancy between intensity- and amplitude-based SHD. As shown in Figs. 2, 3 and 4, amplitude recovery lags behind intensity recovery by 20–40%, a finding quantitatively confirmed in Tables 1 and 2. This discrepancy is rooted in phase distortions: although the overall intensity distribution may resemble the reference beam, residual phase errors prevent full amplitude overlap. As noted by Aiello et al. (2017), this makes amplitude-based SHD the stricter and more realistic measure of robustness, especially for coherent applications (Aiello et al. 2017).

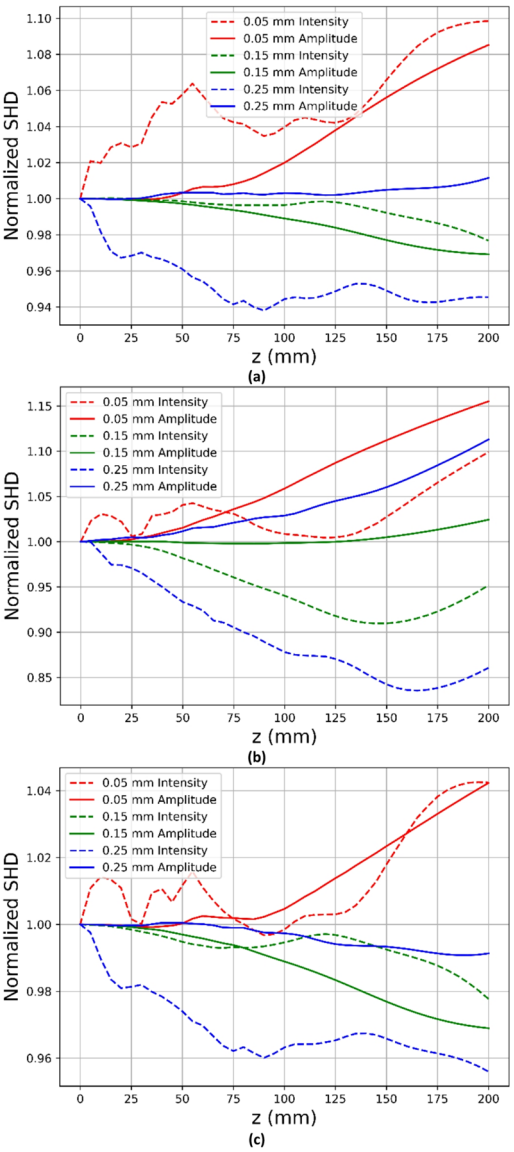


**Fig. 4** The SHD curves for $HG_{22}$ modes obstructed by a **a** disk, **b** vertical strip, and **c** rectangle with different sizes. Red dashed lines correspond to intensity-based similarity; blue solid lines correspond to amplitude-based similarity

It should be noted that the difference between intensity- and amplitude-based similarity originates entirely from the phase distribution of the complex field. Since intensity similarity incorporates only the magnitude of the field, it may indicate apparent recovery even when significant phase distortions persist. In contrast, amplitude-based similarity accounts for both amplitude and phase, making it a more physically meaningful indicator of self-healing, particularly in coherent optical systems. Therefore, in many practical applications, such as holography, interferometry, and coherent communication, phase similarity is more critical than intensity or amplitude similarity, and the lower amplitude-based SHD reported here reflects the incomplete restoration of phase.

**Table 1** Maximum SHD values and recovery distances (in mm) for first- and second-order HG modes under three obstruction types and three obstruction sizes

| Mode | Obstacle | Size (mm) | Intensity | | Amplitude | |
|---|---|---|---|---|---|---|
| | | | $SHD_{max}$ | z (mm) | $SHD_{max}$ | z (mm) |
| $HG_{01}$ | Disk | 0.05 | 1.020 | 200 | 1.102 | 200 |
| | | 0.15 | 1 | 0 | 1.073 | 200 |
| | | 0.25 | 1.012 | 5 | 1.046 | 200 |
| | Strip | 0.05 | 1.086 | 200 | 1.165 | 200 |
| | | 0.15 | 1.033 | 25 | 1.029 | 200 |
| | | 0.25 | 1.554 | 200 | 1.030 | 200 |
| | Rectangle | 0.05 | 1.078 | 200 | 1.113 | 200 |
| | | 0.15 | 1.009 | 5 | 1.052 | 200 |
| | | 0.25 | 1.007 | 5 | 1.048 | 200 |
| $HG_{10}$ | Disk | 0.05 | 1.020 | 200 | 1.102 | 200 |
| | | 0.15 | 1 | 0 | 1.073 | 200 |
| | | 0.25 | 1.012 | 5 | 1.046 | 200 |
| | Strip | 0.05 | 1 | 0 | 1.133 | 200 |
| | | 0.15 | 1.002 | 5 | 1.068 | 200 |
| | | 0.25 | 1.011 | 5 | 1.041 | 200 |
| | Rectangle | 0.05 | 1 | 0 | 1.123 | 200 |
| | | 0.15 | 1.004 | 5 | 1.066 | 200 |
| | | 0.25 | 1.015 | 5 | 1.052 | 200 |
| $HG_{11}$ | Disk | 0.05 | 1.002 | 200 | 1.053 | 200 |
| | | 0.15 | 1 | 0 | 1.103 | 200 |
| | | 0.25 | 1.002 | 5 | 1.047 | 165 |
| | Strip | 0.05 | 1 | 0 | 1.149 | 200 |
| | | 0.15 | 1.002 | 5 | 1.108 | 200 |
| | | 0.25 | 1.013 | 5 | 1.069 | 200 |
| | Rectangle | 0.05 | 1 | 0 | 1.105 | 200 |
| | | 0.15 | 1.004 | 5 | 1.086 | 200 |
| | | 0.25 | 1.011 | 5 | 1.065 | 200 |

### 3.3 Comparative analysis across obstruction types

Tables 1 and 2 summarize the maximum SHD values and the corresponding recovery distances for all modes, obstruction types, and obstruction sizes. These results underscore the interplay between beam structure and obstruction geometry. Circular disks, being symmetric, produce predictable trends: higher-order modes recover more effectively, with $HG_{22}$ showing the strongest resilience. Strip obstructions interact more selectively with mode symmetry. Here, $HG_{11}$ outperforms both $HG_{10}$ and $HG_{01}$, as its diagonal nodal line coincides with the blocked region, effectively "absorbing" the obstruction with less net energy loss. This highlights a geometry-mode alignment principle: obstructions overlapping with nodal regions reduce damage to the beam's coherent structure.

Rectangular fringes consistently yield the weakest SHD. Although intensity snapshots suggest partial recovery, the tabulated SHD values confirm that this is largely illusory. The incoherent diffraction sidelobes created by the fringe resemble lobes of higher-order modes but do not restore the original field. Consequently, SHD values for fringe obstructions often remain close to unity even after long propagation distances, and they show weaker true

**Table 2** Maximum SHD values and recovery distances (in mm) for third- and fourth-order HG modes under three obstruction types and three obstruction sizes

| Mode | Obstacle | Size (mm) | Intensity | | Amplitude | |
|---|---|---|---|---|---|---|
| | | | $SHD_{max}$ | z (mm) | $SHD_{max}$ | z (mm) |
| $HG_{12}$ | Disk | 0.05 | 1.014 | 200 | 1.089 | 200 |
| | | 0.15 | 1.003 | 5 | 1.042 | 200 |
| | | 0.25 | 1.004 | 5 | 1.008 | 200 |
| | Strip | 0.05 | 1.004 | 200 | 1.163 | 200 |
| | | 0.15 | 1.002 | 5 | 1.162 | 200 |
| | | 0.25 | 1.027 | 10 | 1.162 | 200 |
| | Rectangle | 0.05 | 1 | 0 | 1.091 | 200 |
| | | 0.15 | 1.001 | 5 | 1.033 | 200 |
| | | 0.25 | 1.005 | 5 | 1.002 | 55 |
| $HG_{21}$ | Disk | 0.05 | 1.014 | 200 | 1.089 | 200 |
| | | 0.15 | 1.003 | 5 | 1.042 | 200 |
| | | 0.25 | 1.004 | 5 | 1.008 | 200 |
| | Strip | 0.05 | 1.026 | 50 | 1.101 | 200 |
| | | 0.15 | 1 | 0 | 1 | 0 |
| | | 0.25 | 1 | 0 | 1.014 | 200 |
| | Rectangle | 0.05 | 1.029 | 55 | 1.080 | 200 |
| | | 0.15 | 1.004 | 5 | 1.013 | 200 |
| | | 0.25 | 1.001 | 5 | 1.040 | 200 |
| $HG_{22}$ | Disk | 0.05 | 1.099 | 200 | 1.085 | 200 |
| | | 0.15 | 1 | 15 | 1 | 0 |
| | | 0.25 | 1 | 0 | 1.012 | 200 |
| | Strip | 0.05 | 1.099 | 200 | 1.155 | 200 |
| | | 0.15 | 1 | 0 | 1.024 | 200 |
| | | 0.25 | 1 | 0 | 1.113 | 200 |
| | Rectangle | 0.05 | 1.043 | 195 | 1.042 | 200 |
| | | 0.15 | 1 | 0 | 1 | 0 |
| | | 0.25 | 1 | 0 | 1 | 40 |

recovery compared with disks. This finding underscores the necessity of quantitative metrics: visual inspection alone may overestimate the degree of self-healing.

It is worth noting that higher-order HG modes naturally expand over a larger transverse area. As a result, when a fixed-size obstruction is applied, it blocks a smaller fraction of their total intensity compared with lower-order modes. Part of the apparently stronger self-healing observed for modes such as $HG_{21}$ and $HG_{22}$ can therefore be attributed to this difference in effective beam size.

At the same time, the broader angular spectrum of higher-order modes provides additional spatial-frequency components that actively contribute to reconstruction after obstruction, indicating that their enhanced recovery is not solely a geometric effect. A fully normalized comparison, where the obstruction size is scaled relative to the beam area, would help isolate these two contributions more clearly.

Our results extend and refine the understanding of self-healing in structured beams. Early work on Bessel and Airy beams highlighted dramatic self-healing effects (Broky et al. 2008; Durnin 1987), but quantitative comparison across conditions was lacking. Wen and Chu proposed similarity measures for Gaussian-derived beams, yet without normalization, their

results could not account for varying obstruction strengths (Wen and Chu 2015). The introduction of normalized SHD by Saadati-Sharafeh et al. provided a rigorous, transferable framework (Saadati-Sharafeh et al. 2023), which we have applied here for the first time to a systematic study of HG beams.

Zhao et al. studied obstructed HG modes and reported self-healing and transformation effects, but without quantitative normalization (Zhao et al. 2023). Our analysis provides a comprehensive, mode-resolved dataset showing how obstruction size, geometry, and mode order combine to influence recovery. Furthermore, the explicit contrast between amplitude- and intensity-based metrics confirms Aiello et al.'s prediction that amplitude recovery lags behind intensity reconstruction (Aiello et al. 2017), thereby offering a stricter and more realistic measure of robustness.

The simulations demonstrate that higher-order HG beams, particularly $HG_{22}$, are significantly more resilient to partial obstruction than first-order modes. Their broader angular spectrum ensures that missing content can be replenished more effectively, resulting in higher maximum SHD values and longer ranges of useful reconstruction. This suggests that high-order HG beams could be strategically chosen in free-space optical systems where beam clipping or shadowing is unavoidable.

At the same time, the persistent discrepancy between intensity and amplitude SHD underscores a cautionary point. For applications such as imaging, where intensity fidelity suffices, HG modes can indeed be considered robust. However, for tasks requiring phase integrity, such as holography, interferometry, or coherent optical communication, intensity recovery is an inadequate measure. In these contexts, amplitude-based SHD should be used to evaluate performance, as it more accurately reflects the residual distortions that affect information-carrying capacity.

Finally, the dependence of recovery efficiency on the relative alignment between obstacle geometry and mode structure suggests a new design principle: matching the nodal lines of the beam to predictable obstructions can improve resilience. For example, in environments where vertical wires or slits are common, modes like $HG_{11}$ may outperform others due to their natural diagonal nodal line. Such insights provide a practical pathway to engineering structured light that is not only tailored for information capacity but also optimized for robustness in realistic optical channels.

## 4 Conclusions

In this study, we have presented a systematic and quantitative analysis of the self-healing phenomenon in HG beams. By examining six representative modes under three classes of obstructions and evaluating their recovery using both intensity- and amplitude-based normalized similarity measures, we have established a comprehensive picture of how beam order, obstruction size, and geometry jointly determine resilience. The results show that higher-order modes such as $HG_{22}$ consistently outperform their lower-order counterparts, while geometry-mode alignment can enhance recovery in specific cases, as demonstrated by the robustness of $HG_{11}$ under strip-shaped obstructions. At the same time, rectangular fringes yield minimal recovery, reminding us that visual impressions of beam restoration must be treated with caution and supported by rigorous metrics.

A critical outcome of this work is the recognition that amplitude-based self-healing is systematically weaker than intensity-based recovery, often by as much as 20–40%. This finding confirms that while beams may appear to heal in terms of intensity, their phase coherence, and thus their usefulness in coherent optical applications, remains compromised. These insights not only advance our fundamental understanding of beam self-healing but also provide practical guidelines for designing resilient structured beams for optical communication, imaging, and quantum information systems.

**Acknowledgements** Not applicable.

**Author contributions** The authors contributed equally to this work.

**Funding** Not applicable.

**Data availability** The data are available from the corresponding author upon reasonable request.

## Declarations

**Conflict of interest** The authors declare no financial or commercial conflict of interest.

**Ethical approval** Not applicable.

**Consent to participate** Not applicable.

**Consent for publication** Not applicable.

## References

Aiello, A., Agarwal, G.S., Paúr, M., Stoklasa, B., Hradil, Z., Řeháček, J., De La Hoz, P., Leuchs, G., Sánchez-Soto, L.L.: Unraveling beam self-healing. Opt. Express. **25**(16), 19147–19157 (2017)

Angelsky, O.V., Bekshaev, A.Y., Hanson, S.G., Zenkova, C.Y., Mokhun, I.I., Zheng, J.: Structured light: ideas and concepts. Front. Phys. **8**, 114 (2020)

Arrizón, V., Aguirre-Olivas, D., Mellado-Villaseñor, G., Chávez-Cerda, S.: Self-healing in scaled propagation invariant beams. arXiv:1503.03125 (2015)

Ast, S., Di Pace, S., Millo, J., Pichot, M., Turconi, M., Christensen, N., Chaibi, W.: Higher-order Hermite-Gauss modes for gravitational waves detection. Phys. Rev. D. **103**(4), 042008 (2021)

Bandres, M.A., Gutiérrez-Vega, J.C.: Ince–Gaussian modes of the paraxial wave equation and stable resonators. J. Opt. Soc. Am. A. **21**(5), 873–880 (2004)

Beijersbergen, M.W., Allen, L., Van der Veen, H.E., Woerdman, J.P.: Astigmatic laser mode converters and transfer of orbital angular momentum. Opt. Commun. **96**(1–3), 123–132 (1993)

Broky, J., Siviloglou, G.A., Dogariu, A., Christodoulides, D.N.: Self-healing properties of optical airy beams. Opt. Express **16**(17), 12880–12891 (2008)

Chabou, S., Bencheikh, A.: Elegant Gaussian beams: Nondiffracting nature and self-healing property. Appl. Opt. **59**(32), 9999–10006 (2020)

Chu, X., Wen, W.: Quantitative description of the self-healing ability of a beam. Opt. Express. **22**(6), 6899–6904 (2014)

Durnin, J.J.: Exact solutions for nondiffracting beams. I. The scalar theory. J. Opt. Soc. Am. A. **4**(4), 651–654 (1987)

Forbes, A.: Structured light from lasers. Laser Photonics Rev. **13**(11), 1900140 (2019)

Forbes, A., De Oliveira, M., Dennis, M.R.: Structured light. Nat. Photonics. **15**(4), 253–262 (2021)

Goodman, J.W.: Introduction to Fourier Optics. Roberts and Company, Greenwood Village (2005)

Gutiérrez-Vega, J.C., Bandres, M.A.: Helmholtz–Gauss waves. J. Opt. Soc. Am. A. **22**(2), 289–298 (2005)

Hofer, L.R., Jones, L.W., Goedert, J.L., Dragone, R.V.: Hermite–Gaussian mode detection via Convolution neural networks. J. Opt. Soc. Am. A. **36**(6), 936–943 (2019)
Kogelnik, H., Li, T.: Laser beams and resonators. Appl. Opt. **5**(10), 1550–1567 (1966)
Nimavat, A., Sah, A., Pokhra, T., Tripathi, A., Gupta, S.: Analysis of Hermite-Gaussian and Laguerre–Gaussian modes in mode division multiplexing based FSO system. Optoelectron. Adv. Mater.-Rapid Commun. **17**, 122–128 (2023)
Otte, E., Denz, C.: Optical trapping gets structure: structured light for advanced optical manipulation. Appl. Phys. Rev. **7**(4), 041308 (2020)
Saadati-Sharafeh, F., Amiri, P., Akhlaghi, E.A., Azizian-Kalandaragh, Y.: A new criterion for self-healing quantification of structured light beams. J. Opt. **25**(3), 035604 (2023)
Shen, Y., Pidishety, S., Nape, I., Dudley, A.: Self-healing of structured light: A review. J. Opt. **24**(10), 103001 (2022)
Siegman, A.E.: Lasers. University Science Books, Melville (1986)
Sundin, E.M., Navarro, G., Li, C.: Modulated high-order Hermite-Gaussian beams with uniform intensity distribution. Opt. Commun. **554**, 130217 (2024)
Uren, R., Beecher, S., Smith, C.R., Clarkson, W.A.: Method for generating high purity Laguerre–Gaussian vortex modes. IEE J. Quantum Electron. **55**(5), 1–9 (2019)
Voelz, D.G.: Computational Fourier optics: a MATLAB tutorial. (No Title). 4:51 (2011)
Wen, W., Chu, X.: Quantitative comparison of self-healing ability between Bessel–Gaussian beam and airy beam. Ann. Phys. **360**, 549–555 (2015)
Xu, Z., Liu, X., Chen, Y., Wang, F., Liu, L., Monfared, Y.E., Ponomarenko, S.A., Cai, Y., Liang, C.: Self-healing properties of Hermite-Gaussian correlated Schell-model beams. Opt. Express. **28**(3), 2828–2837 (2020)
Zhao, S., Zhang, Z., Wang, X., Chen, J., Gao, Y., Wang, X., Jie, Y., Zhao, C.: Universal Understanding of self-healing and transformation of complex structured beams based on eigenmode superposition. Appl. Opt. **62**(12), 3186–3196 (2023)
Zhou, Y., Zhao, J., Shi, Z., Hashemi Rafsanjani, S.M., Mirhosseini, M., Zhu, Z., Willner, A.E., Boyd, R.W.: Hermite–Gaussian mode sorter. Opt. Lett. **43**(21), 5263–5266 (2018)